Modeling of Hysteresis Loops using Rational and Power Functions

Mehran Mirzaei, Pavel Ripka, Jan Vyhnanek, Andrey Chirtsov and Vaclav Grim

Faculty of Electrical Engineering, Czech Technical University
Prague 16627, Czech Republic, e-mail: mirzameh@fel.cvut.cz

***Abstract*—Simple and precise hysteresis models with a small number of parameters allowing fast calculation are required for the magnetic analysis, as the field is calculated in a very large number of points. This paper presents a new simple method for modeling the hysteresis loops of soft magnetic materials using combined rational and power functions. Three approaches are used to model the hysteresis loops analytically. In the first approach, the upper and lower curves of the hysteresis loops are estimated and are calculated separately, using combined rational and power functions. In the second approach, the hysteresis loops are calculated using the DC magnetization curve and combined rational and power functions, applying a phase shift in the magnetic field strength variations relative to the magnetic flux density. The third approach presents a novel method for modeling hysteresis loops: first, the model is fitted to the "mean curve", which is in the middle of the measured hysteresis curve, and as a second step the phase shift is calculated as in the second approach. A solid iron sample with a rectangular cross section is used for the measurements and the hysteresis modeling. The proposed method is also applied to model the hysteresis loops of a magnetic material with high magnetic permeability and grain-oriented steel, to show the generality of the proposed methods.**

***Keywords*—Hysteresis loops, modeling, combined rational and power functions, analytical**

I. Introduction

Analyzing the magnetic characteristics of soft magnetic materials is the key to the evaluation and design of electromagnetic devices. For example, the hysteresis loop effects in the impedance of solid irons and steels for current carrying busbars and high-permeability magnetic materials are critical for the performance of magnetic sensors, and they should be considered and analyzed in the design process [1]-[3]. Hysteresis loop models are used to analyze electromagnetic devices in transient and steady state analysis [4]-[5].

Various methods for hysteresis loop modeling of magnetic materials have been presented and their appropriateness are compared [6]. Preisach method for hysteresis modeling is well described in [7].It is based on the phenomenological and mathematical modeling method and not a physical based method. It can accurately model major and minor hysteresis loops with high accuracy. Jiles-Atherton method and energetic model are physical based and they depend on micromagnetic characteristics of the magnetic materials [8]-[10].For example, a comparison between Preisach and Jiles-Atherton for hysteresis modeling was presented in [11], which shows extensive measurements requirements for parameters identifications using Preisach model with less problems for precise fitting with measurements. Jiles-Atherton method has opposite properties. However, time-consuming procedures are required to calculate the constants and parameters in [6]-[15], and they are not easy handling for fast design and analysis process and optimization of the magnetic devices. Straightforward and uncomplicated analytical equations and procedures were implemented in [16]-[18]. However, these methods did not show generality of the proposed analytical functions for different magnetic materials. Detailed analyses of hysteresis loops for high magnetic permeability materials and grain-oriented steel laminations were presented in [19]-[21], in which multi-form mathematical functions are used to fit analytical hysteresis loops for various magnetic field strength ranges.

Combined rational and power functions were used in [22] to model magnetization characteristics without hysteresis. In this paper, we present three methods for introducing hysteresis into such a model. The aim is to keep the approximation very simple, so that the model has only minimum parameters and is suitable for design and calculation. The measured hysteresis loops of construction solid iron sample with a rectangular cross section are modeled and shown. The calculated phase shift between the magnetic flux density and the magnetic field strength is applied to calculate the phase angle of the solid iron impedance. The hysteresis loops of a high-permeability magnetic material and grain-oriented steel are also modeled in this paper to show the generality of the proposed method.

II. Measurement of Hysteresis Loops

A compensated permeameter is used to measure DC magnetization and the *B-H* curve and hysteresis loops for a rectangular solid iron sample (Fig. 1). A compensated permeameter is an instrument for measuring hysteresis loops for an open sample at DC and low frequency [23]. A solid iron sample with a rectangular cross section (5 mm · 30 mm) is used for the measurements and for hysteresis modeling. Four hysteresis loop measurements are presented with maximum magnetic field strengths of 500 A/m, 1000 A/m, 3000 A/m and

6000 A/m, respectively. The measured DC magnetization curve for a solid iron sample is shown in Fig. 2.

III. Mathematical Approach

The analytical function of the magnetization or magnetic flux density B versus the magnetic field strength H curve in (1) can be represented as in (2) and (3), using combined rational and power functions [22]:

$$B = J + \mu_0 . H \tag{1}$$

$$f(x) = \left(\left(\sum_{i=1,2,\dots} a_i \cdot x^{b_i} \right) \Big/ \left(1 + \sum_{i=1,2,\dots} c_i \cdot x^{b_i} \right) \right)^{b_0},$$
$$J = f(x), x = H \tag{2}$$

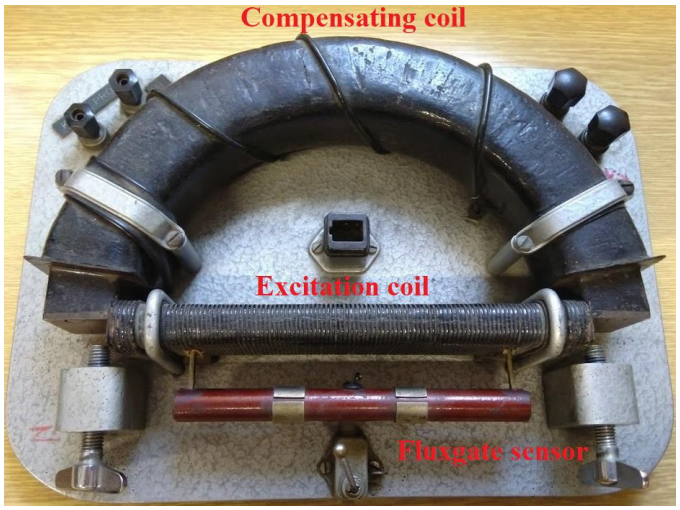

Fig. 1. A DC compensated permeameterand its elements (compensating coil, excitation coil, Fluxgate sensor)

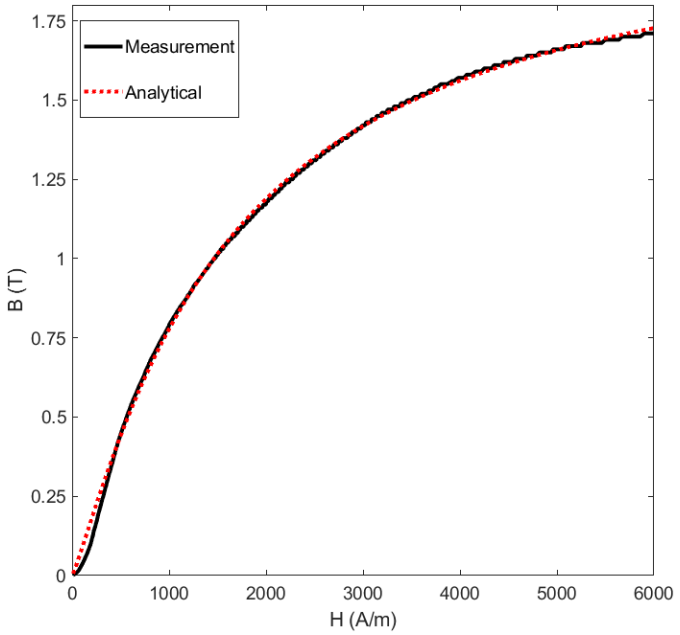

Fig. 2. DC magnetization curve for solid iron - Measurements using permeameter and analytical curve fit using function in (4)

$$f(x) = \left(\sum_{i=1,2,\dots} a_i \cdot x^{b_i} / (1 + c_i \cdot x^{b_i}) \right)^{b_0}, J = f(x), x = H$$
$$f(x) = \left(\sum_{i=1,2,\dots} a_i \cdot x^{b_i} / (1 + c_i \cdot x)^{b_i} \right)^{b_0}, J = f(x), x = H \tag{3}$$

where a_i, c_i and b_i are constants which are calculated using curve fitting, and μ_0 is the magnetic permeability of the free space. Parameter $b_0$is considered to be equal to 1 in this paper. Term $\mu_0 \cdot H$ in (1)-(3) is negligible and it is not considered for the curve fitting because of the low magnetic fields (< 10000 A/m) in modeling the hysteresis loops.

IV. Modeling of Hysteresis Loops

In this paper, first order combined rational and power functions for modeling a DC magnetization curve are only used as follows in two forms of (4) and (5), which also take into account the change in the polarity of the magnetization curve for positive and negative values of the magnetic flux density and the magnetic field strength.

$$B = a_1 \cdot H \cdot |H|^{b_1 - 1} / (c_1 \cdot |H|^{b_1} + 1) \tag{4}$$

$$B = a_1 \cdot H \cdot |H|^{b_1 - 1} / (c_1 \cdot |H| + 1)^{b_1} \tag{5}$$

A. First approach

In the first approach to the modeling of hysteresis loops, the upper and lower curves of the hysteresis loops are calculated separately as described in appendix A, using the proposed functions in (6) - (9). Four parameters, a_1, a'_1, b_1 and c_1, are constants, and they are calculated by curve fitting.

$$B_a = a_1 \cdot H \cdot |H|^{b_1 - 1} / (c_1 \cdot |H|^{b_1} + 1) - a'_1 \cdot (|H_m|^{b_1} - |H|^{b_1}) / (c_1 \cdot |H|^{b_1} + 1) \tag{6}$$

$$B_a = a_1 \cdot H \cdot |H|^{b_1 - 1} / (c_1 \cdot |H|^{b_1} + 1) + a'_1 \cdot (|H_m|^{b_1} - |H|^{b_1}) / (c_1 \cdot |H|^{b_1} + 1) \tag{7}$$

$$B_a = a_1 \cdot H \cdot |H|^{b_1 - 1} / (c_1 \cdot |H| + 1)^{b_1} - a'_1 \cdot (|H_m|^{b_1} - |H|^{b_1}) / (c_1 \cdot |H| + 1)^{b_1} \tag{8}$$

$$B_a = a_1 \cdot H \cdot |H|^{b_1 - 1} / (c_1 \cdot |H| + 1)^{b_1} + a'_1 \cdot (|H_m|^{b_1} - |H|^{b_1}) / (c_1 \cdot |H| + 1)^{b_1} \tag{9}$$

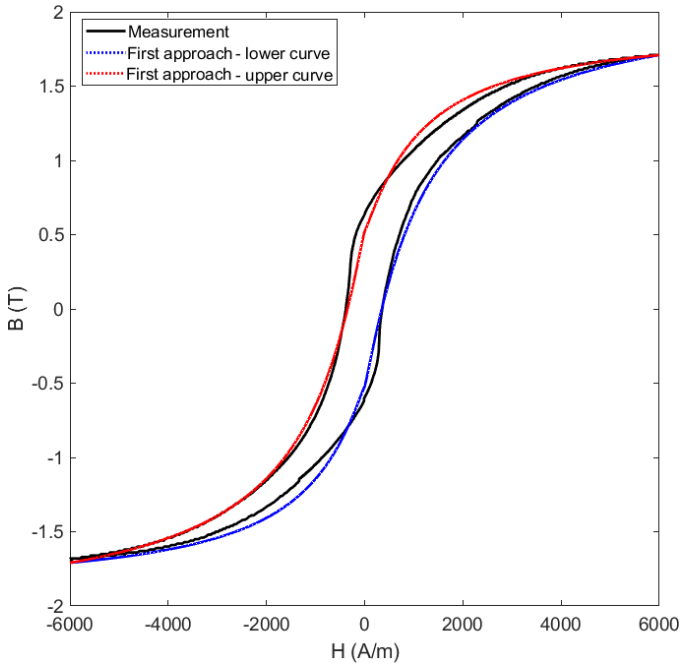

Fig. 3. Hysteresis loop modeling for solid iron (H_m = 6000 A/m) - Measurements using permeameter and analytical curve using second approach in (6) and (7)

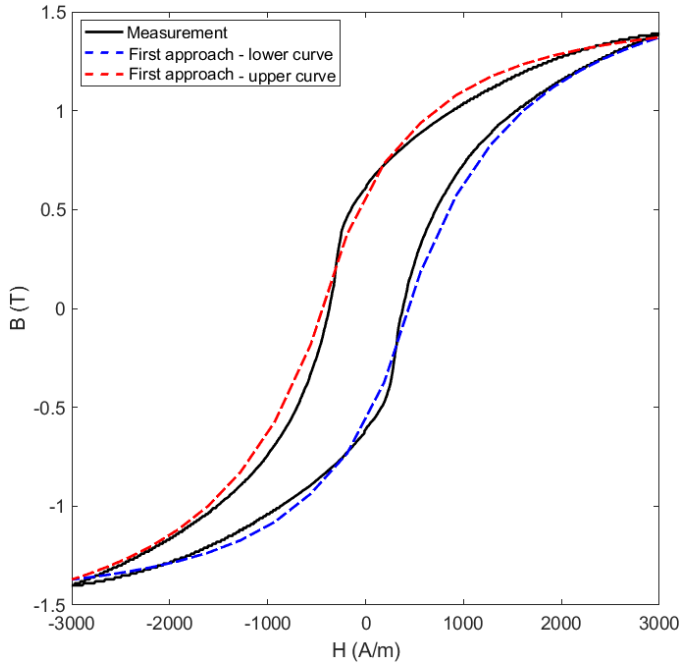

Fig. 4. Hysteresis loop modeling for solid iron (H_m = 3000 A/m) Measurements using permeameter and analytical curve using first approach in (6) and (7)

TABLE I. HYSTERESIS LOOPS PARAMTERS FOR THE FIRST APPROACH USING (6) AND (7)

Parameter	Value
$a_1 - H_m$ = 6000 A/m	$7.021 \cdot 10^{-4}$
$b_1 - H_m$ = 6000 A/m	1.122
$c_1 - H_m$ = 6000 A/m	$3.531 \cdot 10^{-4}$
$a'_1 - H_m$ = 6000 A/m	$3.013 \cdot 10^{-5}$
$a_1 - H_m$ = 3000 A/m	$1.999 \cdot 10^{-4}$
$b_1 - H_m$ = 3000 A/m	1.319
$c_1 - H_m$ = 3000 A/m	$1.199 \cdot 10^{-4}$
$a'_1 - H_m$ = 3000 A/m	$1.653 \cdot 10^{-5}$

Fig. 3 and Fig. 4 show a comparison between measurements and analytical model using the first approach. The results of the first approach for hysteresis loop modeling are as much as necessary precise and the results approximately fit with the measurements. The constants of the upper and lower curves in the first approach, using (6) and (7) could be calculated (Table I) using the curve fitting tool and also the iterative method described in appendix B.

B. Second approach

Parameter x in (2) and (3) can be replaced by function $H_m \cdot \cos(\theta - \theta_o)$ to model hysteresis loops, where H_m is the maximum magnetic field strength (Fig. 5), and θ_o is the phase shift. Fig. 5 presents a schematic model of the hysteresis loops using the first order function in (2) or (3) for different phase shifts θ_o and parameter $b_{i=1}$ in (2) or (3). A higher value for parameter b_1 makes the magnetization curve and the hysteresis loops sharper, and a change to phase shift θ_o makes the hysteresis loops wider or narrower. In the second approach, the DC magnetization curve is used as the method shown in Fig. 6, replacing parameter H with the use of $H_m \cdot \cos(\theta - \theta_o)$ in (4) and (5) to obtain (10) and (11). The phase shift θ_o is calculated to minimize the difference between the analytical model of the hysteresis loops and the measurements.

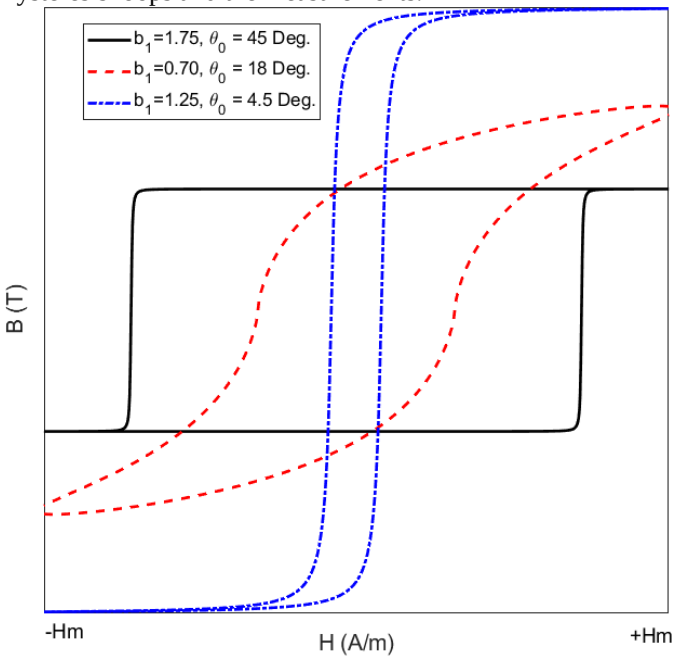

Fig. 5. Schematic models of hysteresis loops for different phase shifts, $\theta_o$modeled by analytical function in (4)

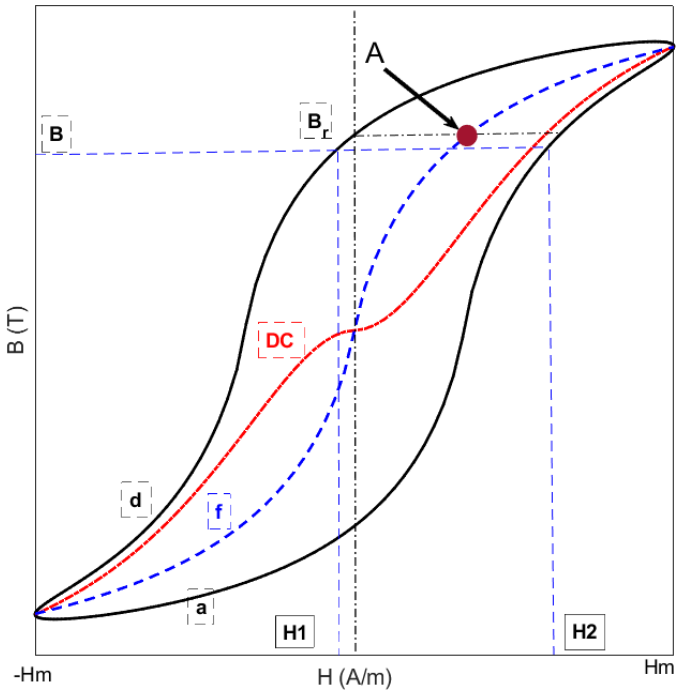

Fig. 6. Schematic model of the hysteresis loop and DC magnetization curvemodeled by analytical function in (4)

$$B = a_1 \cdot H_m \cdot \cos(\theta - \theta_o) \cdot |H_m \cdot \cos(\theta - \theta_o)|^{b_1 - 1} / (c_1 \cdot |H_m \cdot \cos(\theta - \theta_o)|^{b_1} + 1) \quad -\pi \le \theta \le \pi \tag{10}$$

$$B = a_1 \cdot H_m \cdot \cos(\theta - \theta_o) \cdot |H_m \cdot \cos(\theta - \theta_o)|^{b_1 - 1} / (c_1 \cdot |H_m \cdot \cos(\theta - \theta_o)| + 1)^{b_1} \tag{11}$$

Constants a_1, b_1 and c_1 in (4) for the DC magnetization curve (analytical), shown in Fig. 2, are calculated as $4.528 \cdot 10^{-4}$, 1.145 and $2.150 \cdot 10^{-4}$, respectively. The constants in a_1, b_1 and c_1 in (5) are calculated to be equal to $9.827 \cdot 10^{-5}$, 1.439 and $9.556 \cdot 10^{-4}$, respectively. An excellent fit between the measurements and the analytical model for the DC magnetization curve is shown in Fig. 2, except where the field values are very low. The results for hysteresis modeling are shown in Fig. 7 and Fig. 8. The phase shift angle θ_o in the second approach is calculated as 4.0 Deg. and 7.5 Deg. for the maximum magnetic field strength, 6000 A/m and 3000 A/m, respectively. The hysteresis loops for lower fields have bigger phase shifts between the magnetic flux density and the strength of the magnetic field. Both the first approach and the second approach have limited precision, especially for hysteresis loops at lower magnetic field strengths.

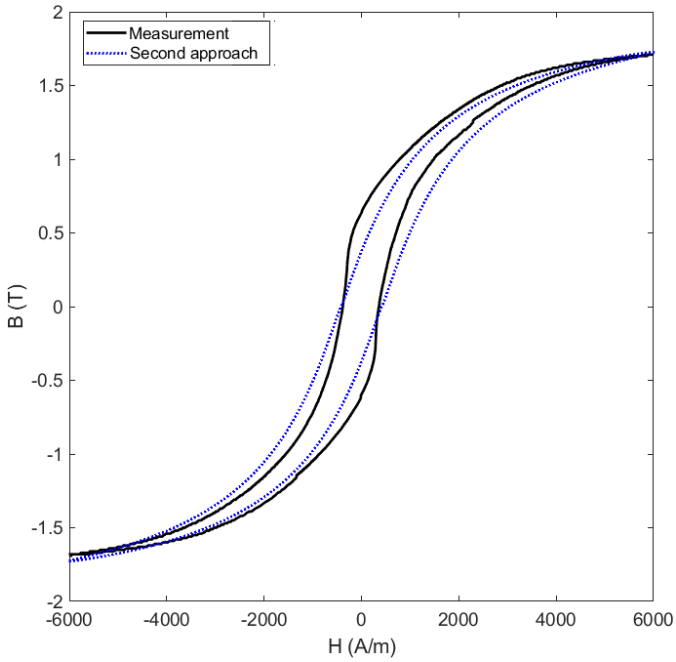

Fig. 7. Hysteresis loop modeling for solid iron (H_m = 6000 A/m) - Measurements using permeameter and analytical curve using second approach in (10)

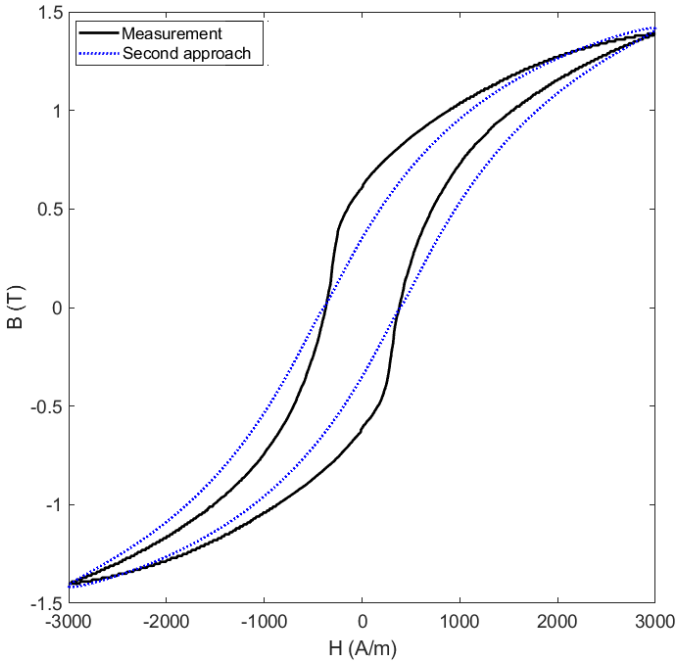

Fig. 8. Hysteresis loop modeling for solid iron (H_m = 3000 A/m) - Measurements using permeameter and analytical curve using second approach in (10)

C. *Third approach*

The third approach to hysteresis loop modeling in this paper uses "mean curve f", which is the average of the rising and falling branches of the hysteresis curve $H_f(B) = (H_a(B) + H_d(B))/2$, as shown in Fig. 6. As a second step, an analytical function in (4) or (5) is fitted to curve f; and finally the phase shift is calculated to this curve to model the hysteresis:

$$B_f = B_a = B_d$$
$$H_f = (H_a + H_d)/2 \quad (12)$$

Fig. 9 - Fig. 12 show a comparison between measurements and third approach models for different maximum values of the strength of the magnetic field. The third approach provides more precise models than the first and second approaches. The calculated constants of (10) and the phase shift angles are presented in Table II for different maximum values of the magnetic field strength, using curve fitting and minimizing the difference between the measurements and the models of hysteresis loops. The hysteresis loop modeling fits better with the measurements at higher maximum magnetic field strengths, H_m = 6000 A/m and 3000 A/m (Fig. 9 and Fig. 10).

The measurements are less symmetric at lower H_m = 1000 A/m and 500 A/m, which causes the greater visual difference in Fig. 9 and Fig. 10. Equation (13) replaces parameter $H_m \cdot \cos(\theta - \theta_o)$ in (10) with parameter $H = H_m \cdot \cos(\theta)$, which is easier to handle for the analysis. The upper and lower curves of the hysteresis loops can be distinguished: the plus sign (+) in (13) corresponds to the upper curve of the hysteresis loop (downward magnetization), and the minus sign (-) corresponds to the lower curve (upward magnetization). Calculations of hysteresis losses can be made using (13), as the upward and downward magnetization curves are separated.

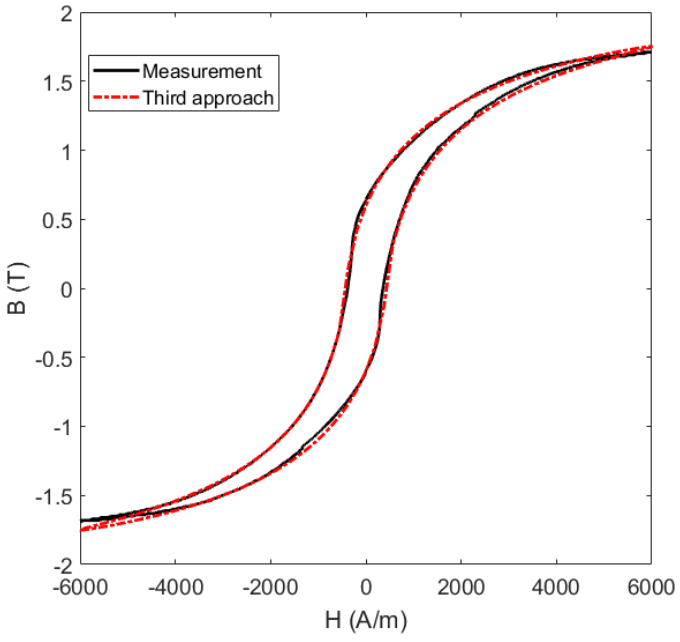

Fig. 9. Hysteresis loop modeling for solid iron (H_m = 6000 A/m) - Measurements using permeameter and analytical curve using third approach in (10)

$$H_m \cdot \cos(\theta - \theta_o) = H_m \cdot (\cos(\theta) \cdot \cos(\theta_o) + \sin(\theta) \cdot \sin(\theta_o)) = H_m \cdot \left(\cos(\theta) \cdot \cos(\theta_o) \pm \sqrt{1 - (\cos(\theta))^2} \cdot \sin(\theta_o)\right) = H \cdot \cos(\theta_o) \pm \sqrt{H_m^2 - H^2} \cdot \sin(\theta_o),\ H = H_m \cdot \cos(\theta),\ -H_m \le H \le +H_m \quad (13)$$

Appendix B shows simple iterative methods to calculate parameters of the hysteresis models for first and third approaches.

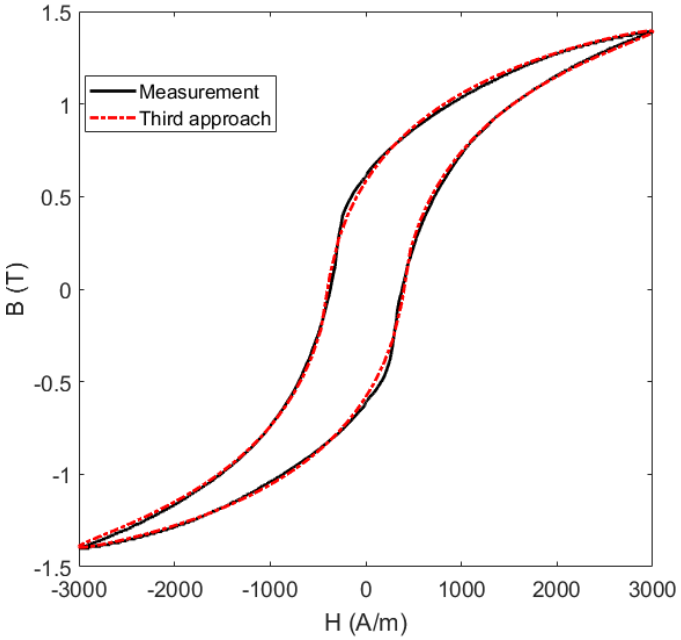

Fig. 10. Hysteresis loop modeling for solid iron (H_m = 3000 A/m) - Measurements using permeameter and analytical curve using third approach in (10)

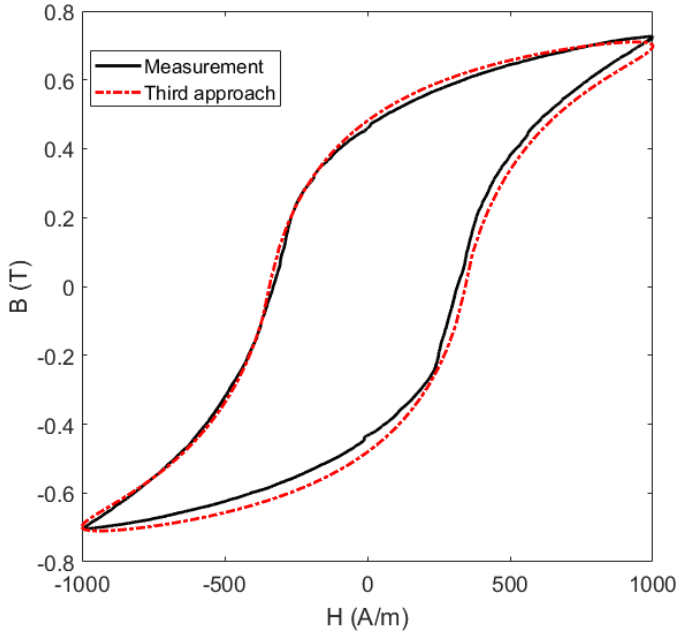

Fig. 11. Hysteresis loop modeling for solid iron (H_m = 1000 A/m) - Measurements using permeameter and analytical curve using third approach in (10)

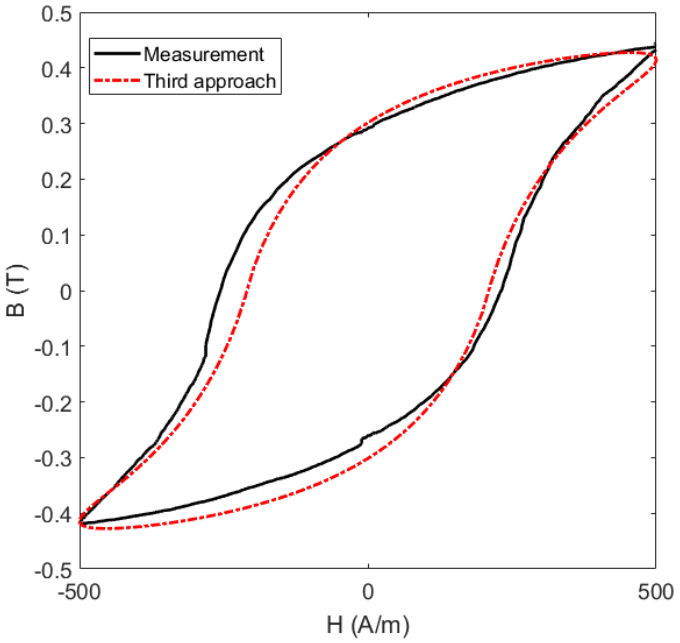

Fig. 12. Hysteresis loop modeling for solid iron (H_m = 500 A/m) - Measurements using permeameter and analytical curve using third approach in (10)

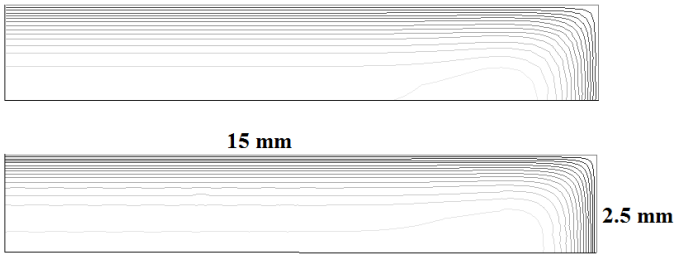

Fig. 13. Magnetic flux distribution in one quarter of a rectangular solid conductor- without hysteresis (above)and with hysteresis (below)

The first and third approach for hysteresis modeling show better accuracy than the second approach. However, more hysteresis loop input data are required for the first and third approaches. The first approach can be used when there is no access to hysteresis loop data.

TABLE II. HYSTERESIS LOOPS PARAMTERS FOR THE THIRD APPROACH USING (10)

Parameter	Value
$a_1 - H_m$ = 6000 A/m	$9.472 \cdot 10^{-3}$
$b_1 - H_m$ = 6000 A/m	0.7315
$c_1 - H_m$ = 6000 A/m	$3.678 \cdot 10^{-3}$
$\theta_o - H_m$ = 6000 A/m	4.0 Deg.
$a_1 - H_m$ = 3000 A/m	$1.04 \cdot 10^{-2}$
$b_1 - H_m$ = 3000 A/m	0.7211
$c_1 - H_m$ = 3000 A/m	$4.347 \cdot 10^{-3}$
$\theta_o - H_m$ = 3000 A/m	7.5 Deg.
$a_1 - H_m$ = 1000 A/m	$6.104 \cdot 10^{-3}$
$b_1 - H_m$ = 1000 A/m	0.855
$c_1 - H_m$ = 1000 A/m	$5.872 \cdot 10^{-3}$
$\theta_o - H_m$ = 1000 A/m	20 Deg.
$a_1 - H_m$ = 500 A/m	$4.044 \cdot 10^{-3}$
$b_1 - H_m$ = 500 A/m	0.9236
$c_1 - H_m$ = 500 A/m	$6.245 \cdot 10^{-3}$
$\theta_o - H_m$ = 500 A/m	24.8

V. IMPEDANCE ANALYSIS OF SOLID IRON BUSBAR

The effect of hysteresis on the internal impedances of a solid iron conductor is considerable and it must be taken into account, as shown in [1] and [24]. Impedance angle θ_z in (14) is dependent on the phase shift angle θ_o between B and H. Table III shows a comparison of the impedance angles between measurements and simulations. H_o is the strength of the magnetic field on the circumference of a rectangular solid iron conductor, which is calculated by the applied current I, the rectangular conductor cross section thickness t, and the width w, in (15).

The magnetic flux distribution in one quarter of a rectangular solid conductor is shown in Fig. 13, with and without taking hysteresis into consideration, showing the difference, especially in the middle of the conductor.

$$Z = R + jX, \theta_z = arctan(X/R) \quad (14)$$

$$H_o = 0.5\, I/(t + w) \quad (15)$$

TABLE III. IMPEDANCE PHASE ANGLE

Parameter	Value
$\theta_Z - H_o$ = 500 A/m (Exp.)	31.66 Deg.
$\theta_Z - H_o$ = 500 A/m (FEM without hysteresis)	43.58 Deg.
$\theta_Z - H_o$ = 500 A/m (FEM with hysteresis)	30.78 Deg.
$\theta_Z - H_o$ = 1000 A/m (Exp.)	31.43 Deg.
$\theta_Z - H_o$ = 1000 A/m (FEM without hysteresis)	43.49 Deg.
$\theta_Z - H_o$ = 1000 A/m (FEM with hysteresis)	32.92 Deg.

It is essential to take the hysteresis angle into consideration in internal impedance calculations, as presented in Table III. The impedance angle θ_z in (14) decreases by about 12 Deg., which causes a lower inductive part or inductance, and a higher resistive part or resistance.

VI. HIGH MAGNETIC PERMEABILITY MATERIAL

A highly magnetic permeability material, Vitrovac 6025X [25], is also considered for hysteresis modeling. The calculated constants of (10) and (11) are presented in Table IV and Table V. The phase shift angle is calculated as 10.9 Deg. The modeled hysteresis loop shows noteworthy accuracy (Fig. 14) for high magnetic permeability materials, despite the less-than-perfect symmetrical measured hysteresis loop. The values of parameter b_1 in Tables IV and V are higher than for solid iron in Table II, due to the higher permeability. The phase shift angle is considerably smaller than for solid iron at the same maximum magnetic flux density value of about 0.5 T, as high-quality magnetic materials have narrow hysteresis loops in order to have lower iron and hysteresis losses.

TABLE IV. HYSTERESIS LOOP PARAMTERS FOR THE THIRD APPROACH – USING (10)

Parameter	Value
a_1	0.2439
b_1	1.103
c_1	0.4363
θ_o	10.9 Deg.

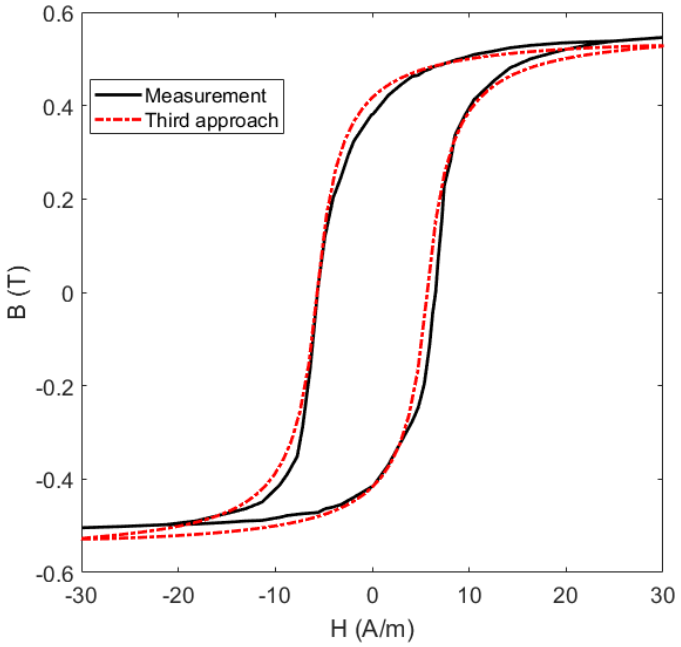

Fig. 14. Hysteresis loops modeling for high magnetic permeability material (H_m = 30 A/m) - Measurements [25] and analytical curve using third approach in (10)

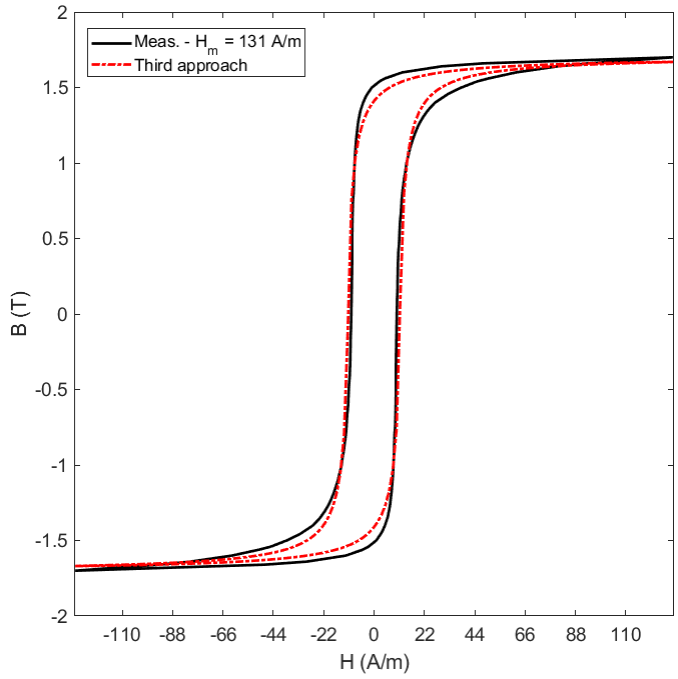

Fig. 15. Hysteresis loops modeling for grain oriented steel(H_m = 131 A/m) - Measurements [26] and analytical curve using third approach in (10)

TABLE V. HYSTERESIS LOOP PARAMTERS FOR THE THIRD APPROACH – USING (11)

Parameter	Value
a_1	0.2963
b_1	1.212
c_1	0.5783
θ_o	10.9 Deg.

VII. GRAIN ORIENTED STEEL

Hysteresis loops of grain-oriented steel are modeled using the third approach. Table VI presents the calculated parameters of hysteresis loops at various values of H_m. Fig. 15- Fig. 18 show modeled hysteresis loops in comparison with the values presented in [26]. Modeled hysteresis loops could be better fitted with the use of higher order combined rational and power functions, but this would substantially increase the computation time.

TABLE VI. HYSTERESIS LOOPS PARAMTERS FOR THE THIRD APPROACH USING (10)

Parameter	Value
$a_1 - H_m$ = 131 A/m	0.9282
$b_1 - H_m$ = 131 A/m	0.8899
$c_1 - H_m$ = 131 A/m	0.5429
$\theta_o - H_m$ = 131 A/m	5.0 Deg.
$a_1 - H_m$ = 38 A/m	0.312
$b_1 - H_m$ = 38 A/m	1.349
$c_1 - H_m$ = 38 A/m	0.2006
$\theta_o - H_m$ = 38 A/m	13.9 Deg.
$a_1 - H_m$ = 21 A/m	0.2124
$b_1 - H_m$ = 21 A/m	1.378
$c_1 - H_m$ = 21 A/m	0.1438
$\theta_o - H_m$ = 21 A/m	20 Deg.
$a_1 - H_m$ = 14 A/m	0.1519
$b_1 - H_m$ = 14 A/m	1.403
$c_1 - H_m$ = 14 A/m	0.1257
$\theta_o - H_m$ = 14 A/m	24.0

The maximum differences are seen for the hysteresis loop with H_m = 131 A/m. This is because of the different phase shift in the hysteresis loops for low value fields, for medium value field ranges and for high value field ranges. The differences could be reduced by using a variable phase shift instead of a constant phase shift for the hysteresis loop for high fields, which is planned for future work. The value of parameter b_1 goes down from low fields to high fields because the magnetization curve has sharper changes in the low fields.

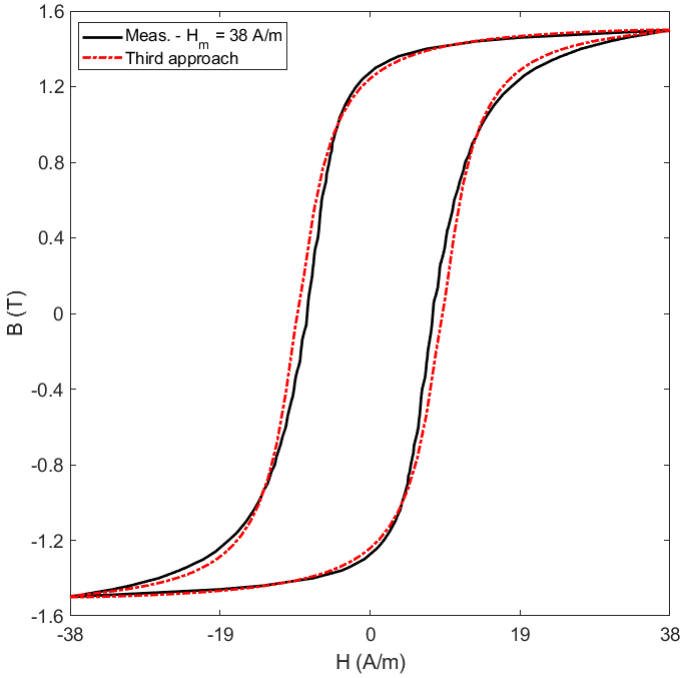

Fig. 16. Hysteresis loops modeling for grain oriented steel(H_m = 38 A/m) - Measurements [26] and analytical curve using third approach in (10)

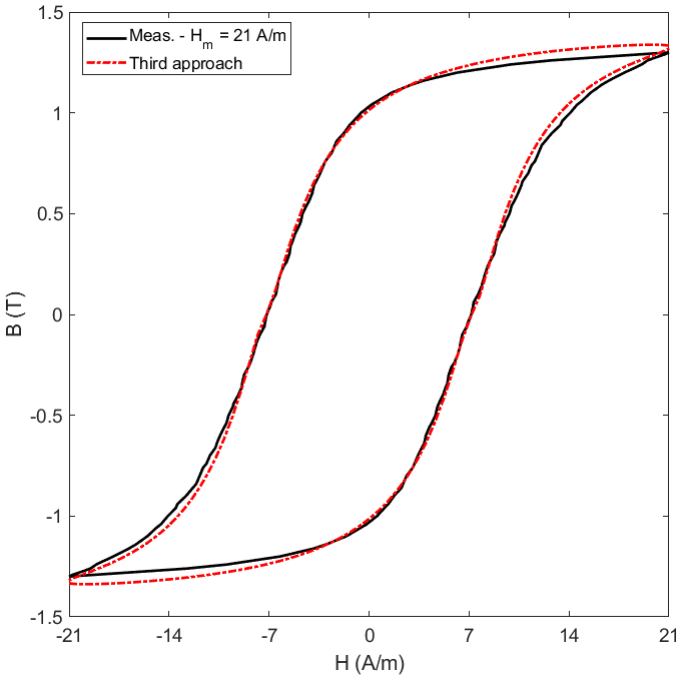

Fig. 17. Hysteresis loops modeling for grain oriented steel(H_m = 21 A/m) - Measurements [26] and analytical curve using third approach in (10)

VIII. Discussions

Calculated phase shift, θ_o (Tables II and VI) curve versus magnetic field strength, H for solid iron and grain-oriented steel are shown in Fig. 19 and Fig. 20. They show the maximum phase shift corresponds to the maximum relative magnetic permeability, which confirms same conclusion in [24], [27].

The presented hysteresis modeling using third approach is fast and precise, which is crucial for electromagnetic devices analysis [28]-[33] with less time-consuming process.

Micromagnetic models can simulate soft and hard magnetic materials [34]-[35] at very small scale and find magnetic domains with exact physical basis.

Hysteresis loop models including micromagnetic and physical parameters are ideal for understanding of the magnetization processes [36]-[37]. Such models are available, but they have complicated curve fitting [38]. The disadvantage of these methods is that they are very time consuming and therefore less practical for magnetic materials in macroscopic range [39].

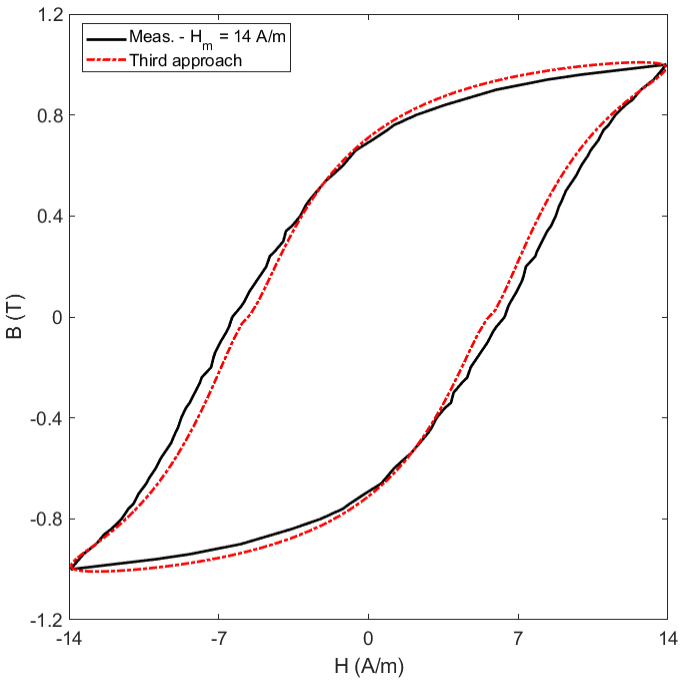

Fig. 18. Hysteresis loops modeling forgrain oriented steel (H_m = 14 A/m) - Measurements [26] and analytical curve using third approach in (10)

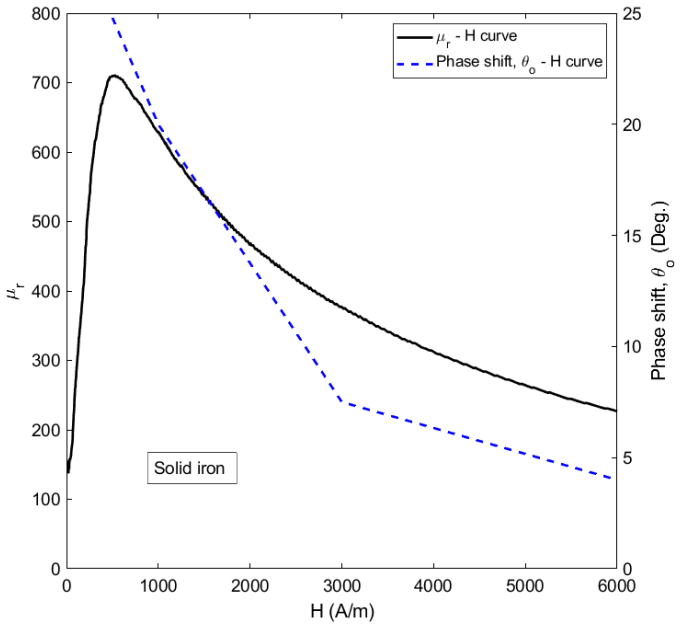

Fig. 19. Relative magnetic permeability, μ_r curve versus magnetic field strength, H and phase shift angle, θ_o curve versus H– solid iron

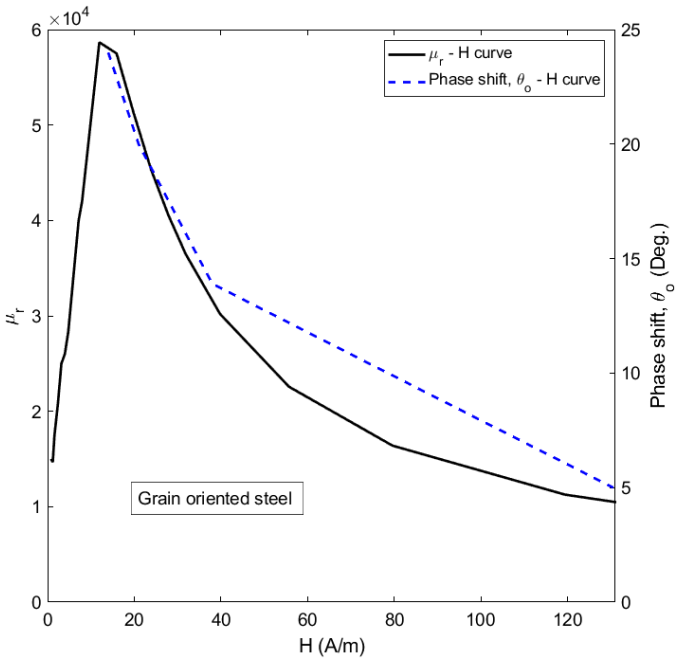

Fig. 20. Relative magnetic permeability, μ_r curve versus magnetic field strength, H and phase shift angle, θ_o curve versus H– Grain oriented steel

Finding relationship between constants and maximum magnetic field strength, H_m of hysteresis loop of the proposed approach for hysteresis modeling is essential for electromagnetic calculations with direct consideration of hysteresis loops [40]-[41]. The main reason is that ~~As~~ hysteresis loops from measuremets are ~~is not~~ usually available only for few values of H_m. ~~for any maximum magnetic field strength.~~ ~~, for example, from measurements.~~ Functions of constants, a_1, b_1, c_1 and θ_o versus maximum magnetic field strength of hysteresis loop for third approach are presented in Appendix C. It is shown that relationship between constants, a_1, b_1, c_1 and θ_o could be linear and rational functions.

IX. Conclusions

The proposed analytical methods for hysteresis loop modeling utilize a single closed-form equation for the entire B-H loop, which is simpler to implement than multi-function modeling of hysteresis loops. It has been shown that the methods presented for hysteresis modeling are a good compromise between simplicity and high accuracy. The third approach to modeling hysteresis loops is the most precise method, and it is very suitable for fast hysteresis modeling. Modeling can be made also using known physical parameters H_c, B_r, H_m and B_m as shown in Appendix B. The generality of the proposed method for various magnetically soft materials has been demonstrated on construction iron, grain-oriented steel and high-permeability amorphous alloy magnetic materials. Greater precision could be obtained with higher order combined rational and power functions, but this would increase the computational time.

Calculating the phase shift between magnetic flux density B and magnetic field strength H is essential for resistance and inductance analysis of solid iron busbars in power systems, as it has a big influence on the phase angle of the impedance.

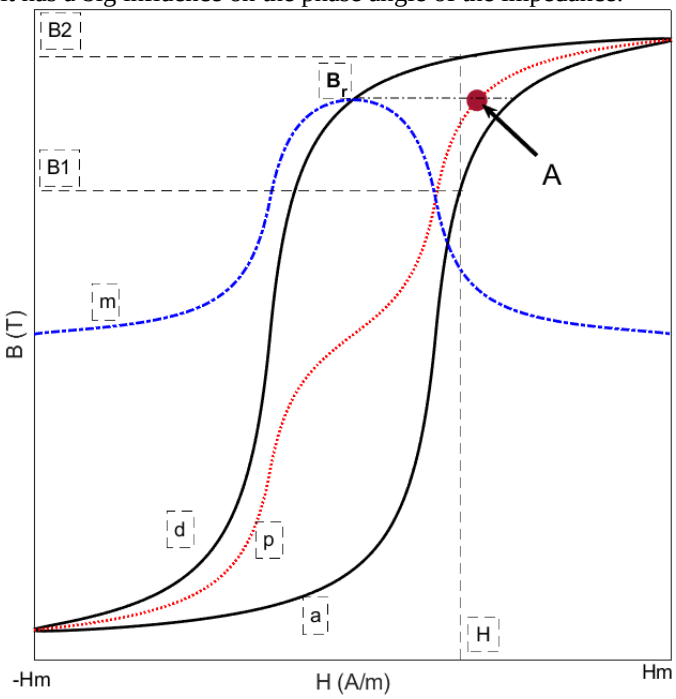

Fig. 21. Schematic model of the hysteresis loop used in first approachmodeled by analytical function in (6) and (7)

X. Appendix A

Two auxiliary curves, p and m (Fig. 21) in (16) are extracted from curves corresponding to rising (lower) and falling (upper) curves, a and d of hysteresis loops [16]. Functions in (17) – (20) are assumed for the mathematical modeling of the curves p and m.

$$H_p = H_m = H_a = H_d$$
$$B_p = (B_d + B_a)/2$$
$$B_m = (B_d - B_a)/2$$
$$B = B_p \pm B_m \quad (16)$$

$$B_p = a_1 \cdot H \cdot |H|^{b_1-1}/(c_1 \cdot |H|^{b_1} + 1) \quad (17)$$

$$B_m = a_1' \cdot (|H_m|^{b_1} - |H|^{b_1})/(c_1 \cdot |H|^{b_1} + 1) \quad (18)$$

$$B_p = a_1 \cdot H \cdot |H|^{b_1-1}/(c_1 \cdot |H| + 1)^{b_1} \quad (19)$$

$$B_m = a_1' \cdot (|H_m|^{b_1} - |H|^{b_1})/(c_1 \cdot |H| + 1)^{b_1} \quad (20)$$

XI. Appendix B

An alternative method for calculating of the constants of the first approach in (6) and (7) is using equations in (21)-(24). Equations (21)-(23) correspond to the three points (0, $\pm B_r$), ($\pm H_c$, 0) and ($\pm B_m$, $\pm H_m$) in a hysteresis loop, which are obvious points in any hysteresis loop. H_c, B_r and B_m are coercivity force, remanence and the maximum flux density of the hysteresis loop corresponding to the maximum magnetic field strength, H_m, respectively. Another equation is required to calculate four

constants,a_1, b_1, c_1 and a'_1, which corresponds to the differential permeability, $\mu_{r\text{-}d\text{-}A}$ in point A,(H_A, B_r) of Fig. 21. Point (H_A, B_r) in the curve p corresponds to the remanence magnetic flux density, B_r.

A simple numerical procedure is used to calculate constants, a_1, b_1, c_1 and a'_1. Firstly, initial value 1 is considered for the constant, b_1. Constant, a'_1 is calculated using (21) in second step. Equation (22) is used to obtain constant, a_1 in third step with calculated value, a'_1 from second step. Calculated constant, a_1 from (22) is replaced in (23) to obtain constant, c_1 in fourth step. Constant, b_1 is recalculated using (24) and calculated constants, a_1, c_1 and a'_1 in previous steps. The final and converged values of constants, a_1, b_1, c_1 and a'_1 could be calculated after 10 to 20 iterations, which takes less than 1 second time for the calculations. Fig. 22 shows hysteresis loop modeling of solid iron using first approach with calculated constants, a_1, b_1, c_1 and a'_1in Table VII as described in (21)-(24).

$$(0, \pm B_r) \rightarrow B_r = a_1' \cdot |H_m|^{b_1}, a_1' = B_r/|H_m|^{b_1} \tag{21}$$

$$(\pm H_c, 0) \rightarrow 0 = a_1 \cdot |H_c|^{b_1}/(c_1 \cdot |H_c|^{b_1} + 1) - a_1' \cdot (|H_m|^{b_1} - |H_c|^{b_1})/(c_1 \cdot |H_c|^{b_1} + 1)$$
$$a_1 = a_1' \cdot (|H_m|^{b_1}/|H_c|^{b_1} - 1) \tag{22}$$

$$(\pm H_m, \pm B_m) \rightarrow B_m = a_1 \cdot |H_m|^{b_1}/(c_1 \cdot |H_m|^{b_1} + 1)$$
$$c_1 = a_1 \cdot 1/B_m - 1/|H_m|^{b_1} \tag{23}$$

$$B_p = a_1 \cdot H \cdot |H|^{b_1 - 1}/(c_1 \cdot |H|^{b_1} + 1)$$
$$\mu_{r-d}\mu_0 = dB_p/dH = a_1 \cdot b_1 \cdot |H|^{b_1 - 1}/(c_1 \cdot |H|^{b_1} + 1)^2$$
$$b_1 = \mu_{r-d-A}\mu_0 \cdot (c_1 \cdot |H_A|^{b_1} + 1)^2/(a_1 \cdot |H_A|^{b_1 - 1}) \tag{24}$$

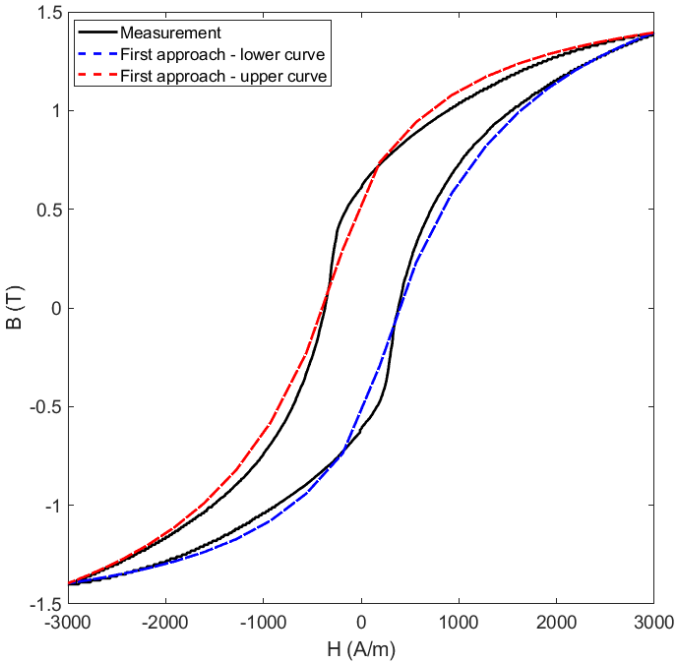

Fig. 22. Hysteresis loop modeling for solid iron (H_m = 3000 A/m) - Measurements using permeameter and analytical curve using first approach in (21) -(24)

TABLE VII. HYSTERESIS LOOPS PARAMTERS FOR THE FIRST APPROACH USING (21) AND (24) -FIG. 22

Parameter	Value
$a_1 - H_m$ = 3000 A/m	$7.0134 \cdot 10^{-4}$
$b_1 - H_m$ = 3000 A/m	1.1222
$c_1 - H_m$ = 3000 A/m	$3.7749 \cdot 10^{-4}$
$a'_1 - H_m$ = 3000 A/m	$7.6792 \cdot 10^{-5}$

Also the alternative approach to the curve fitting method for calculating four constants a_1, b_1, c_1 and $\theta_o$of third approach in (10) has similar numerical procedure as first method in (21)-(24), which are presented in four equations in (25) - (28).In order to calculate the phase shift, θ_o, the phase angle, θ_c is calculated according to (25). The phase shift, θ_o is obtained with condition in (26). The initial values of the parameters a_1 and c_1 are calculated from (27) with consideration of initial value 1 for b_1, which correspond to two points (H_m, B_m) and (H_A, B_r) in Fig. 6. Constant, b_1 is recalculated using (28) and calculated constants, $a_1$and $c_1$in previous steps. The differential permeability, $\mu_{r\text{-}d\text{-}A}$ corresponds to point A, (H_A, B_r) of Fig. 6. The final and converged values of constants, a_1, b_1 and c_1 could be calculated after 10 to 20 iterations. Fig. 23 and Fig. 24 show hysteresis loop modeling of solid iron and grain oriented steel using third approach with calculated constants, a_1, b_1, c_1 and θ_o in Tables VIII and IX as described in (25)-(28).

$$H = H_c = H_m \cdot cos(\theta_c), \theta_c = -\cos^{-1}(H_c/H_m), -\pi \leq \theta \leq 0$$
$$H = -H_c = H_m \cdot cos(\theta_c), \theta_c = \pi - \cos^{-1}(H_c/H_m), 0 \leq \theta \leq \pi \tag{25}$$

$$B(H = H_c) = 0$$
$$B = a_1 \cdot H_m \cdot cos(\theta_c - \theta_o) \cdot |H_m \cdot \cos(\theta_a - \theta_o)|^{b_1 - 1}/(c_1 \cdot |H_m \cdot \cos(\theta_a - \theta_o)|^{b_1} + 1) = 0$$
$$\rightarrow \theta_c - \theta_o = -\pi/2 \rightarrow \theta_o = \pi/2 + \theta_c = \pi/2 - \cos^{-1}(H_c/H_m) \tag{26}$$

$$B_m = a_1 \cdot |H_m|^{b_1}/(c_1 \cdot |H_m|^{b_1} + 1)$$
$$B_r = a_1 \cdot |H_A|^{b_1}/(c_1 \cdot |H_A|^{b_1} + 1)$$
$$a_1 = B_m \cdot B_r/(B_r - B_m) \cdot (1/|H_m|^{b_1} - 1/|H_A|^{b_1})$$
$$c_1 = 1/(B_r - B_m) \cdot (B_m/|H_m|^{b_1} - B_r/|H_A|^{b_1}) \tag{27}$$

$$B_f = a_1 \cdot H \cdot |H|^{b_1 - 1}/(c_1 \cdot |H|^{b_1} + 1)$$
$$\mu_{r-d}\mu_0 = dB_f/dH = a_1 \cdot b_1 \cdot |H|^{b_1 - 1}/(c_1 \cdot |H|^{b_1} + 1)^2$$
$$b_1 = \mu_{r-d-A} \cdot \mu_0 \cdot (c_1 \cdot |H_A|^{b_1} + 1)^2/(a_1 \cdot |H_A|^{b_1 - 1}) \tag{28}$$

TABLE VIII. HYSTERESIS LOOPS PARAMTERS FOR THE THIRD APPROACH USING (25)-(28) – FIG. 23

Parameter	Value
$a_1 - H_m$ = 500 A/m	$5.728 \cdot 10^{-3}$
$b_1 - H_m$ = 500 A/m	0.8407
$c_1 - H_m$ = 500 A/m	$8.017 \cdot 10^{-3}$
$\theta_o - H_m$ = 500 A/m	28.8

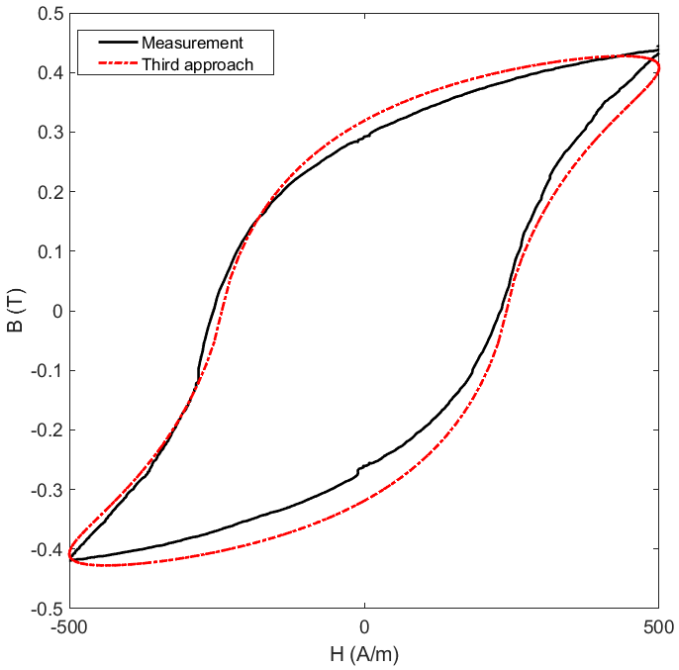

Fig. 23. Hysteresis loop modeling for solid iron (H_m = 500 A/m) - Measurements using permeameter and analytical curve using third approach in (25) - (28)

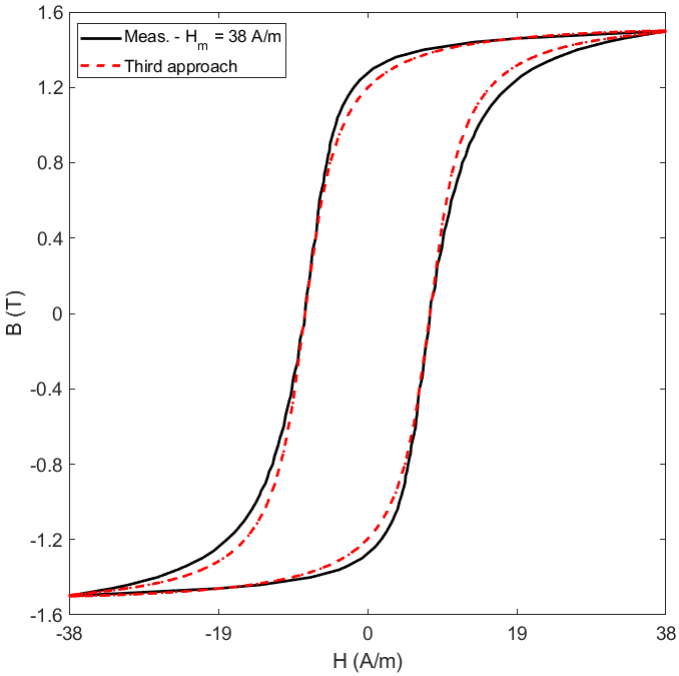

Fig. 24. Hysteresis loops modeling for grain oriented steel (H_m = 38 A/m) - Measurements [26] and analytical curve using third approach in (25) -(28)

TABLE IX. HYSTERESIS LOOPS PARAMTERS FOR THE THIRD APPROACH USING (10) -FIG. 24

Parameter	Value
$a_1 - H_m$ = 38 A/m	0.3774
$b_1 - H_m$ = 38 A/m	1.2581
$c_1 - H_m$ = 38 A/m	0.2414
$\theta_o - H_m$ = 38 A/m	12.0 Deg.

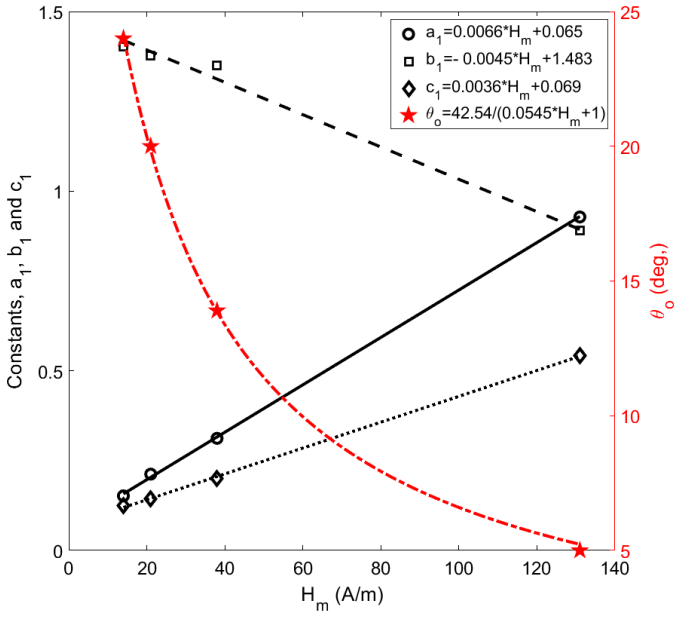

Fig. 25. Constants, a_1, b_1 and c_1 and phase shift, θ_o versus maximum field strength, H_m for grain oriented steel

XII. APPENDIX C

Asd an ~~For~~ example, we calculated functions of constants, a_1, b_1, c_1 and θ_o versus maximum magnetic field strength, H_m for grain oriented steel. ~~are calculated.~~ The relationship between constants, a_1, b_1, and c_1 and H_m could be estimated as linear function as shown in Fig. 25. The functions are a_1=0.0066H_m+0.065, b_1=-0.0045H_m+1.483, and c_1 = 0.0036H_m+0.069.

The hysteresis angle or phase shift angle, θ_o versus H_m could be estimated as a rational function [24], [42]-[43] for H_m larger than $H_{\mu\text{-max}}$, which $H_{\mu\text{-max}}$ corresponds to the maximum relative magnetic permeability (Fig. 19 – Fig. 20). The function is θ_o =42.54/(0.0545H_m+1).

References

[1] M. Mirzaei, P. Ripka, A. Chirtsov, J. Vyhnanek, "Impedance of iron conductors with circular and rectangular shapes," Proceedings of the IECON 2018 - 44th Annual Conference of the IEEE Industrial Electronics Society, Washington, DC, USA, 21-23 October, 2018.

[2] M. Nowicki, R. Szewczyk, T. Charubin, A. Marusenkov, A. Nosenko, V. Kyrylchuk, "Modeling the hysteresis loop of ultra-high permeability amorphous alloy for space applications," Materials (11) (2018) 1-10.

[3] P. Ripka, "Sensors based on bulk soft magnetic materials: Advances and challenges," J. Magn. Magn. Mater. 320 (20) (2008) 2466-2473.

[4] C. Carrander, S. A. Mousavi, G Engdahl, "An application of the time-step topological model for three-phase transformer no-load current calculation considering hysteresis," J. Magn. Magn. Mater., 423, (2017), 241-243.

[5] A. A. Adly and H. H. Hanafy, "Incorporating core hysteresis properties in three-dimensional computations of transformer inrush current forces, " J. Appl. Phys. 105, 07A329 (2009).

[6] A. Ivany, *Hysteresis models in electromagnetic computation*, Akademiai Kiado, Budapest, 1997

[7] I. D. Mayergoyz, *Mathematical models of hysteresis*, New York: Springer-Verlag, 1991.

[8] D.C Jiles and D.L. Atherton, "Theory of ferromagnetic hysteresis," Journal of Applied Physics , vol. 55, no. 6, (1984), 2115-2120

[9] D.C Jiles and D.L. Atherton, "Theory of ferromagnetic hysteresis," J. Magn. Magn. Mater., vol. 61, no. 1-2, (1986), 48-60

[10] H. Hauser, "Energetic model of ferromagnetic hysteresis: Isotropic magnetization," Journal of Applied Physics, vol.96, no.5, (1984), 2753-2767

[11] D. A. Philips, L. R. Dupre, and J. A. Melkebeek, "Comparison of Jiles and Preisach hysteresis models in magnetodynamics," IEEE Trans. Magn., vol. 31, no. 6, (1995), 3551–3553

[12] A. Skarlatos, A. Martínez-de-Guerenu, R. Miorelli, A. Lasaosa, C. Reboud, "Use of meta-modelling for identification and interpolation of parametric hysteresis models applied to the characterization of carbon steels," Physica B: Condensed Matter, 549, (2018), 122–126

[13] S. E. Zirka, Y. I. Moroz, R. G. Harrison, and K. Chwastek, "On physical aspects of the Jiles-Atherton hysteresis models," J. Appl. Phys. 112, 043916 (2012)

[14] A. P. S. Baghel and S. V. Kulkarni, "Hysteresis modeling of the grain-oriented laminations with inclusion of crystalline and textured structure in a modified JilesAtherton model, " J. Appl. Phys. 113, 043908 (2013)

[15] B. Sai Ram, S.V. Kulkarni, "An isoparametric approach to model ferromagnetic hysteresis including anisotropy and symmetric minor loops," J. Magn. Magn. Mater., 474, (2019), 574–584.

[16] J. Rivas, J. M. Zamarro, E. Martin, C. Pereira, "Simple approximation for magnetization curves and hysteresis loops," IEEE Trans. Mag. 17 (4) (1983) 1498-1502.

[17] L. Battistelli, G. Gentile, A. Piccolo, "Representation of hysteresis loops by rational fraction approximations," Physica Scripta. 40, (1989), 502-507.

[18] Z. Wlodarski, "Analytical description of magnetization curves," Physica B, 373, (2006), 323–327.

[19] I. Nova, V. Havlicek, I. Zemanek, "Dynamic hysteresis loops modeling by means of extended hyperbolic model," IEEE Trans. Mag. 49 (1) (2013) 148-151.

[20] I. Nova, I. Zemanek, "Analytical model with flexible parameters for dynamic hysteresis loops modeling," J. of Elec. Eng., 61, (7/s), (2010), 46-49.

[21] I. Nova, I. Zemanek, "Analytical inverse model with flexible parameters for dynamic hysteresis loops modelling,"Prz. Elek. (9b), (2011), 89-92.

[22] M. Mirzaei, P. Ripka, "Analytical functions of magnetization curves for high magnetic permeability materials," IEEE Trans. Mag. 54 (11) (2018).

[23] P. Kaspar, P. Ripka. J. Vyhnanek, "DC compensated permeameter – the accuracy study," J. of Elec. Eng., 69, (6), (2018), 415-417.

[24] D. O'Kelly, "Hysteresis and eddy current losses in steel plates with nonlinear magnetization characteristics," Proc. IEE, 119 (11) (1972) 1675-1676.

[25] J. Kubik, L. Pavel, P. Ripka, P. Kaspar, "Low-power printed circuit board fluxgate sensor," IEEE SENS. J., 7 (2) (2007), 179-183.

[26] D-C Hysteresis loops - M-2 Mill – Anneal GOES 0.007 in. Thick, AK Steel, Available online on 11.09.2018: https://www.aksteel.com › sites › default › files › lite-carlite-and-mill-anneal

[27] D. O'Kelly, "Flux penetration and core loss in solid iron," IEEE Trans. Mag. 11 (1) (1975) 55-60.

[28] Z. Q. Wu, G. H. Shirkoohi, J. Z. Ca, "Simple dynamic hysteresis modelling of three phase power transformer," J. Magn. Magn. Mater., 160, (1996), 79-80.

[29] Z. Sigut, T. Zemcik, "Hysteresis loop analytical approximation," J. Magn. Magn. Mater., 73, (1988), 193-198.

[30] J. Zhao, S. E. Zirka, Y. I. Moroz, T. Matsuo, "Physical Cauer circuits in nonlinear eddy-current modeling," J. Magn. Magn. Mater., 508, (2020), 166850.

[31] Y. Liu, D. Zhang, Z. Li, J. Li, L. Wu, S. Zhang, and H. Tang,"Study of the stray losses calculation in structural parts for HVDC converter transformers based on the TEAM problem 21 family," IEEE Trans. Power. Delivery.31 (2) (2016) 605-612.

[32] J. He, L. Yu, X. Wang, and X. Song,"Simulation of transient skin effect of DC railway system based on MATLAB/Simulink," IEEE Trans. Power. Delivery.28 (2) (2013) 145-152.

[33] H. Lu, A. Bokhari, T. Hong, and F. de Leon, "Experimental evaluation of available computational methods for eddy current and hysteresis losses for cables installed in steel pipes," IEEE Trans. Power. Delivery.33 (4) (2018) 1777-1786.

[34] G. P. Zhao and X. L. Wang, "Nucleation, pinning, and coercivity in magnetic nanosystems: An analytical micromagnetic approach," Phys. Rev. B 74, 012409 (2006)

[35] G. P. Zhao,X. L. Wang, C. Yang, L. H. Xie and G. Zhou, "Self-pinning: Dominant coercivity mechanism in exchange-coupled permanent/composite magnets," J. of App. Phys. 101, 09K102 (2007)

[36] A. Furuya, J. Fujisaki, Y. Uehara, K. Shimizu, H. Oshima, and T. Matsuo, "Micromagnetic hysteresis model dealing with magnetization flip motion for grain-oriented silicon steel," IEEE Trans. Mag., vol. 50, no. 11, (2014)

[37] M. Hofmann, H. Naumoski, U. Herr, and H.-G. Herzog, "Magnetic properties of electrical steel sheets in respect of cutting: micromagnetic analysis and macromagnetic modeling," IEEE Trans. Mag., vol. 52, no. 2, (2016)

[38] D. C. Jiles, J. B. Thoelke. and M. K. Devine, "Numerical determination of hysteresis parameters the modeling of magnetic properties using the theory of ferromagnetic hysteresis," IEEE Trans. Mag., vol. 28, no. 1 (1992), 27-35

[39] F. Liorzou, B. Phelps, and D. L. Atherton, "Macroscopic models of magnetization," IEEE Trans. Mag., vol. 36, no. 2, (2000), 418-428

[40] H. Okama, Y. Takahashi, K. Fujiwara, "A measurement method of minor hysteresis loss of electrical steel sheet bymeans of a single sheet tester," J. Magn. Magn. Mater., 505, (2020) 166688,.

[41] Z. Wlodarski,, "Extraction of hysteresis loops from main magnetization curves," J. Magn. Magn. Mater., 308, (2007) 15-19.

[42] D. O'Kelly, "Fundamental and harmonic flux estimation in a steel plate with a sinusoidal applied field," J. Phys. D: Appl. Phys., 10, (1977), 2107-2115.

[43] D. O'Kelly, "Flux penetration and core loss in solid iron," IEEE Trans. Mag., vol. 11, no. 1 (1975), 55-60